Reduced-Order Adaptive Observer With Asymptotic Stability for Sensorless Control of SPMSM

Jiong Li, Yao Sun, *Member, IEEE*, Jianheng Lin, *Member, IEEE*, Xing Li, Feng Zhou, *Member, IEEE*, and Hanbing Dan, *Senior Member, IEEE*

***Abstract*—The design of the back electromotive force (EMF) observer is important in sensorless speed control of surface-mounted permanent magnet synchronous motors. However, many existing back EMF observers are coupled with the phase-locked loop (PLL), which not only complicates observer design but also poses challenges in ensuring global asymptotic stability. To address this challenge, this article introduces a reduced-order adaptive observer (ROAO) characterized by PLL-independent, which greatly simplifies the parameter design of the observer. In addition, the proposed ROAO is globally asymptotically stable with rigorous proof via the Lyapunov theorem. Finally, the effectiveness of the proposed observer is verified by simulation and experiment.**

***Index Terms*—Reduced-order adaptive observer (ROAO), sensorless control, surface-mounted permanent magnet synchronous motors (SPMSM).**

I. Introduction

PERMANENT magnet synchronous motors (PMSMs) are widely utilized due to their benefits, such as lightweight construction, compact size, high efficiency, and rapid dynamic response [1], [2], [3]. To lower hardware costs and enhance reliability, encoderless control for PMSMs has been extensively investigated [4]. Sensorless speed control schemes are typically categorized into saliency-based sensorless control for low-speed operation and model-based sensorless control for high-speed operation. The saliency-based method involves injecting high-frequency voltage as excitation to extract rotor position information from the current response. However, the injection of high-frequency signals unavoidably leads to additional losses, torque ripple, and acoustic noise [5], [6], [7].

Model-based sensorless control methods can be further subdivided into back electromotive force (EMF)-based and flux-based methods. Typically, the stator flux is estimated using a pure integrator. However, the dc component of the current can saturate the integrator, and the initial value of the integrator can also lead to inaccuracies in flux estimation. Using the low-pass filter (LPF) [8] or disturbance observer [9], [10], [11], [12] can effectively eliminate the dc component, which requires cumbersome parameter tuning due to multiple parameters involved. The authors in [13], [14], and [15] proposed a nonlinear flux observer based on a gradient-descent method, which is globally stable. Since information on magnet flux linkage is necessary for observer design, its performance may degrade when there is an uncertainty in the magnet flux linkage. To improve the robustness, Bobtsov et al.[16] proposed an observer that includes an estimator for the initial value of the magnet flux linkage. Its rotor position estimation error is globally asymptotically stable when the speed meets the persistent excitation (PE) condition.

Back EMF-based sensorless control methods primarily consist of model reference adaptive systems (MRAS) [17], [18], extended Kalman filters (EKF) [19], [20], sliding mode observers (SMO) [21], [22], [23], [24], [25], [26], and extended state observers (ESO) [27], [28], [29], [30], [31], [32]. The rotor speed and position estimation approach based on MRAS is straightforward, while its performance heavily relies on machine parameters [18]. EKF can yield optimal/suboptimal state estimates, featuring noise immunity and parameter robustness [19]. However, this method requires substantial online computation, imposing a significant computational burden. SMO has gained widespread attention in sensorless control due to its simple structure, robustness, and rapid convergence. To mitigate the adverse effects of chattering resulting from switching control, numerous enhanced methods based on SMO have been proposed. Various switching functions are employed to reduce chattering, albeit at the expense of observer robustness [22], [23]. Adaptive SMOs can adjust observer gain according to operating conditions to prevent undesirable chattering induced by excessive gain [24], [25]. In addition, LPF and rotor position compensation can be utilized to alleviate the impact of chattering [33]. ESO is utilized to estimate back EMF as a form of disturbance observer. The authors in[28] and [29] enhanced observer dynamic performance by employing the estimated speed from the phase-locked loop (PLL) to online tune ESO parameters. [30] combines

Received 15 May 2024; revised 14 August 2024; accepted 21 September 2024. Date of publication 24 September 2024; date of current version 12 December 2024. This work was supported in part by the National Natural Science Foundation of China under Grant 62125308, Grant 52337008, Grant 52377183, Grant 52377168, and Grant 52277071, and in part by the Provincial Natural Science Foundation of Hunan under Grant 2022JJ30141. Recommended for publication by Associate Editor I. Slama-Belkhodja. *(Corresponding authors: Yao Sun; Feng Zhou.)*

Jiong Li, Yao Sun, Jianheng Lin, and Hanbing Dan are with the School of Automation, Central South University, Changsha 410083, China, and also with the Hunan Provincial Key Laboratory of Power Electronics Equipment and Grid, Changsha 410083, China (e-mail: 224601002@csu.edu.cn; yaosun@mail.csu.edu.cn; ljhljh@csu.edu.cn; hanbingdan@csu.edu.cn).

Xing Li is with the College of Electrical and Information Engineering, Hunan University, Changsha 410082, China (e-mail: lxhnu@hnu.edu.cn).

Feng Zhou is with the College of Electronic Information and Electrical Engineering, Changsha University, Changsha 410082, China (e-mail: zhoufeng@ccsu.edu.cn).

Color versions of one or more figures in this article are available at https://doi.org/10.1109/TPEL.2024.3466910.

Digital Object Identifier 10.1109/TPEL.2024.3466910

proportional resonant regulator with ESO to mitigate adverse effects of harmonic components on back EMF.

Although back EMF-based sensorless control methods have been widely adopted, the stability analysis of some of these methods remains challenging. For example, there is little work on the stability analysis of ESOs [27], [28], [29], [30]. The main reason is that the estimated speed information from the PLL is needed for the design of these observers, and the stability analysis of the observer cannot be performed independently of the PLL. The adaptive ESOs proposed by the authors in [34] and [35] design adaptive terms to estimate the unknown speed, thereby avoiding the dependence on PLL information. However, only local stability analysis is provided.

In this article, a globally asymptotically stable reduced-order adaptive observe (ROAO) with the PLL-independent feature is designed, which has the following advantages.

1) A ROAO with PLL-independent is introduced, which greatly simplifies the parameter design of the observer.
2) The global asymptotic stability of the proposed ROAO is proved via the Lyapunov theorem.

The rest of this article is organized as follows. Section II gives the existing problems of the conventional back EMF observers. In Section III, the design of the proposed ROAO is presented. Furthermore, the stability of the observer and the guidelines for parameter selection are given in detail. The comparison results of the simulation and experiment are presented in Section IV to verify the feasibility of the observer. Finally, Section V concludes this article.

II. Problems With Conventional Observer

A. Mathematical Model of SPMSM

The voltage equations of surface-mounted permanent magnet synchronous motors (SPMSM) in the stationary frame are as follows:

$$\begin{cases} \frac{di_\alpha}{dt} = -\frac{R_s}{L_s} i_\alpha + \frac{u_\alpha}{L_s} - \frac{e_\alpha}{L_s} \\ \frac{di_\beta}{dt} = -\frac{R_s}{L_s} i_\beta + \frac{u_\beta}{L_s} - \frac{e_\beta}{L_s} \end{cases} \tag{1}$$

where u_α and u_β denote the $\alpha\beta$-axis stator voltages, i_α and i_β are the $\alpha\beta$-axis stator currents, R_s is the stator resistance, L_s is the stator inductance, and e_α and e_β are the $\alpha\beta$-axis back EMFs.

Assuming a uniform air-gap magnetic flux and neglecting the high-order harmonics of the back EMFs, e_α and e_β can be expressed as follows [30]:

$$\begin{cases} e_\alpha = -\psi_f \omega_e \sin\theta_e \\ e_\beta = \psi_f \omega_e \cos\theta_e \end{cases} \tag{2}$$

where ψ_f denotes the magnet flux linkage, ω_e is the electrical angular velocity of the rotor, and θ_e is the rotor electrical position.

B. Conventional Observer Revisit

By defining the state vector $\boldsymbol{x}_l \triangleq \begin{bmatrix} i_\alpha & i_\beta & e_\alpha & e_\beta \end{bmatrix}^T$, the state space model of $\boldsymbol{x}_l$ can be obtained according to (1) and (2) as follows:

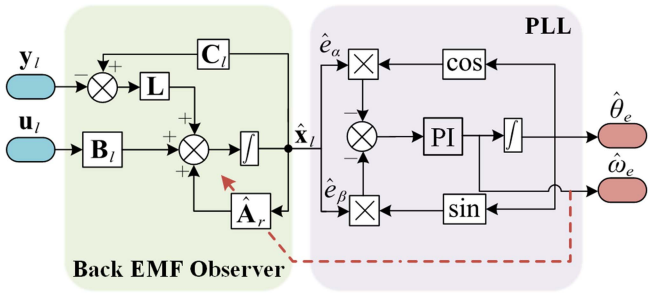

Fig. 1. Structure block diagram of the conventional observer.

$$\begin{cases} \dot{\boldsymbol{x}}_l = \mathbf{A}_l \boldsymbol{x}_l + \mathbf{B}_l \boldsymbol{u}_l \\ \boldsymbol{y}_l = \mathbf{C}_l \boldsymbol{x}_l \end{cases} \tag{3}$$

where $\mathbf{A}_l = \begin{bmatrix} -\frac{R_s}{L_s}\mathbf{I} & -\frac{1}{L_s}\mathbf{I} \\ 0 & \omega_e \mathbf{J} \end{bmatrix}$, $\mathbf{B}_l = \begin{bmatrix} \frac{1}{L_s}\mathbf{I} \\ 0 \times \mathbf{I} \end{bmatrix}$, $\boldsymbol{u}_l = \begin{bmatrix} u_\alpha \\ u_\beta \end{bmatrix}$, $\mathbf{C}_l = \begin{bmatrix} \mathbf{I} \\ 0 \times \mathbf{I} \end{bmatrix}^T$, $\mathbf{I} = \begin{bmatrix} 1 & 0 \\ 0 & 1 \end{bmatrix}$, and $\mathbf{J} = \begin{bmatrix} 0 & -1 \\ 1 & 0 \end{bmatrix}$.

Since the augmented matrix $\begin{bmatrix} \mathbf{C}_l & \mathbf{C}_l\mathbf{A}_l \end{bmatrix}^T$ is a full-rank matrix, the system (3) is observable. The observer for (3) can be designed as follows:

$$\dot{\hat{\boldsymbol{x}}}_l = \hat{\mathbf{A}}_l \hat{\boldsymbol{x}}_l + \mathbf{B}_l \boldsymbol{u}_l + \mathbf{L}\left(\mathbf{C}_l \hat{\boldsymbol{x}}_l - \boldsymbol{y}_l\right) \tag{4}$$

where the superscript "^" denotes the estimated variables, $\hat{\mathbf{A}}_l = \begin{bmatrix} -\frac{R_s}{L_s}\mathbf{I} & -\frac{1}{L_s}\mathbf{I} \\ 0 & \hat{\omega}_e \mathbf{J} \end{bmatrix}$, and $\mathbf{L} = \begin{bmatrix} l_1\mathbf{I} \\ l_2\mathbf{I} \end{bmatrix}$ is the gain matrix of the observer to be designed. The structure block diagram of the conventional observer is shown in Fig. 1.

Subtracting (3) from (4) yields

$$\dot{\tilde{\boldsymbol{x}}}_l = \left(\mathbf{A}_l + \mathbf{L}\mathbf{C}_l\right)\tilde{\boldsymbol{x}}_l + \tilde{\mathbf{A}}_l \hat{\boldsymbol{x}}_l \tag{5}$$

where $\tilde{\boldsymbol{x}}_l = \hat{\boldsymbol{x}}_l - \boldsymbol{x}_l$ is the observation error, $\tilde{\mathbf{A}}_l = \begin{bmatrix} 0 & 0 \\ 0 & \tilde{\omega}_e \mathbf{J} \end{bmatrix}$, and $\tilde{\omega}_e = \hat{\omega}_e - \omega_e$.

Numerous existing works overlook the coupling term $\tilde{\mathbf{A}}_l \hat{\boldsymbol{x}}_l$ with the PLL and simply think that the observer is stable if $\mathbf{A}_l + \mathbf{L}\mathbf{C}_l$ is a Hurwitz matrix [27], [28], [29], [30]. Such a simplification may lay a potential risk to system stability [35]. In addition, the parameter design of the conventional observers is complex due to the coupling between the back EMF observer and the PLL.

III. Proposed Reduced-Order Adaptive Observer

To address the problems of the abovementioned conventional observer, a globally asymptotically stable ROAO with the PLL-independent feature is designed. Different from the conventional EMF observers, the proposed adaptive observer estimates the unknown speed information using an adaptive term, resulting in cascaded structures for the proposed observer and PLL. This structure guarantees the decoupling between the observer and PLL.

Hereafter, two assumptions are made, given as follows.

1) *Studied SPMSM system operates in nonzero speed conditions:* This is a common assumption for back EMF observers, as the amplitude of back EMFs becomes zero and the system becomes unobservable in the zero-speed condition. This limitation can be overcome by the high-frequency injection method.
2) *Derivative of the rotor speed is zero:* This assumption is reasonable because the rate of change of the rotor speed is much smaller than the bandwidth of the back EMF observer [36].

A. Design of Reduced-Order Adaptive Observer

Defining the state vector $\boldsymbol{x}_r \triangleq \begin{bmatrix} e_\kappa & \dot{e}_\kappa \end{bmatrix}$ $(\kappa = \alpha, \beta)$, and the state space model of $\boldsymbol{x}_r$ can be described according to (2) as follows:

$$\begin{cases} \dot{\boldsymbol{x}}_r = \bar{\mathbf{A}}_r \boldsymbol{x}_r \\ y_r = \bar{\mathbf{C}}_r \boldsymbol{x}_r \end{cases} \tag{6}$$

where $\bar{\mathbf{A}}_r = \begin{bmatrix} 0 & 1 \\ -\omega_e^2 & 0 \end{bmatrix}$ and $\bar{\mathbf{C}}_r = \begin{bmatrix} 1 \\ 0 \end{bmatrix}^T$.

The state space model (6) remains the same whether κ is equal to α or β. In the following, an ROAO is designed for the case of $\kappa = \alpha$ estimating the back EMF e_α without using the rotor speed information estimated by the PLL. Clearly, the same ROAO can also be applied to the case of $\kappa = \beta$ estimating the back EMF e_β.

According to (1), the back EMF y_r to be estimated in (6) can be rewritten as follows:

$$y_r = u_\alpha - L_s \dot{i}_\alpha - R_s i_\alpha. \tag{7}$$

To facilitate the design of the adaptive observer, a nonsingular transformation is introduced as follows:

$$\boldsymbol{z}_r = \mathbf{T} \boldsymbol{x}_r \tag{8}$$

where $\mathbf{T}$ is an invertible matrix

$$\mathbf{T} = \frac{1}{k_1^2 + k_2^2 \omega_e^2} \begin{bmatrix} k_1 & -k_2 \\ k_2 \omega_e^2 & k_1 \end{bmatrix} \tag{9}$$

with k_1 and k_2 are positive real numbers to be designed.

Substituting (9) into (8) yields

$$\boldsymbol{x}_r = \mathbf{T}^{-1} \boldsymbol{z}_r = \begin{bmatrix} k_1 z_{r1} + k_2 z_{r2} \\ -k_2 z_{r1} \omega_e^2 + k_1 z_{r2} \end{bmatrix}. \tag{10}$$

It is worth mentioning that ω_e is unavailable in (9) and (10). However, the objective of this section is to estimate the back EMF y_r. According to (10), this objective is achieved as long as the new state vector $\boldsymbol{z}_r$ is estimated.

Substituting (8) into (6), the state space model of $\boldsymbol{z}_r$ can be obtained as follows:

$$\begin{cases} \dot{\boldsymbol{z}}_r = \mathbf{A}_r \boldsymbol{z}_r \\ y_r = \mathbf{C}_r \boldsymbol{z}_r \end{cases} \tag{11}$$

where $\mathbf{A}_r = \mathbf{T} \bar{\mathbf{A}}_r \mathbf{T}^{-1} = \begin{bmatrix} 0 & 1 \\ \varepsilon & 0 \end{bmatrix}$, $\mathbf{C}_r = \bar{\mathbf{C}}_r \mathbf{T}^{-1} = \begin{bmatrix} k_1 \\ k_2 \end{bmatrix}^T$, and $\varepsilon = -\omega_e^2$.

Since the system (11) is observable, according to the certainty equivalence principle of adaptive control, the adaptive observer for (11) can be designed as follows:

$$\dot{\hat{\boldsymbol{z}}}_r = \hat{\mathbf{A}}_r \hat{\boldsymbol{z}}_r + \mathbf{K} \left(\mathbf{C}_r \hat{\boldsymbol{z}}_r - y_r \right) \tag{12}$$

where $\hat{\mathbf{A}}_r = \begin{bmatrix} 0 & 1 \\ \hat{\varepsilon} & 0 \end{bmatrix}$, $\mathbf{K} = \begin{bmatrix} -1/k_2 \\ -k_3 \end{bmatrix}$ is the observer gain matrix with $k_3 > 0$, and $\hat{\varepsilon}$ is the adaptive term to be estimated.

Substituting (7) into (12), the adaptive observer can be rewritten as follows:

$$\dot{\hat{\boldsymbol{z}}}_r = \hat{\mathbf{A}}_r \hat{\boldsymbol{z}}_r + \mathbf{K} \mathbf{C}_r \hat{\boldsymbol{z}}_r + L_s \mathbf{K} \dot{i}_\alpha - \mathbf{K} u_\alpha + R_s \mathbf{K} i_\alpha. \tag{13}$$

To avoid using the information about stator current derivatives in the observer, a new state vector is defined as follows:

$$\boldsymbol{\xi} \triangleq \boldsymbol{z}_r - L_s \mathbf{K} i_\alpha. \tag{14}$$

According to (7) and (11), the state space model of ξ is obtained as follows:

$$\dot{\boldsymbol{\xi}} = \left(\mathbf{A}_r + \mathbf{K} \mathbf{C}_r \right) \boldsymbol{\xi} + L_s \mathbf{A}_r \mathbf{K} i_\alpha - \mathbf{K} \left(u_\alpha - L_s \mathbf{C}_r \mathbf{K} i_\alpha - R_s i_\alpha \right). \tag{15}$$

Proposition 1: If the information of stator resistance and stator inductance is known, according to the certainty equivalence principle of adaptive control, the adaptive observer for (15) can be designed as follows:

$$\dot{\hat{\boldsymbol{\xi}}} = \underbrace{\left(\hat{\mathbf{A}}_r + \mathbf{K} \mathbf{C}_r \right) \hat{\boldsymbol{\xi}} + L_s \hat{\mathbf{A}}_r \mathbf{K} i_\alpha - \mathbf{K} \left(u_\alpha - L_s \mathbf{C}_r \mathbf{K} i_\alpha - R_s i_\alpha \right)}_{\hat{\boldsymbol{\xi}}_d} \tag{16}$$

where $\hat{\boldsymbol{\xi}}_d$ denotes the right-hand side of (16), and the updated law of the adaptive term $\hat{\varepsilon}$ in $\hat{\mathbf{A}}_r$ is given as follows:

$$\begin{cases} \hat{\varepsilon} = \chi - \gamma L_s i_\alpha \hat{\xi}_1 + \dfrac{\gamma L_s^2}{2k_2} i_\alpha^2 \\ \dot{\chi} = -\gamma \left(\mathbf{C}_r \hat{\boldsymbol{\xi}} - u_\alpha + R_s i_\alpha + L_s \mathbf{C}_r \mathbf{K} i_\alpha \right) r(t) + \gamma L_s i_\alpha \bar{\mathbf{C}}_r \hat{\boldsymbol{\xi}}_d \\ r(t) = \hat{\xi}_1 - \dfrac{L_s}{k_2} i_\alpha \end{cases} \tag{17}$$

where $\gamma > 0$ is the adaptive gain for $\hat{\varepsilon}$.

The observation error of ROAO $\tilde{\boldsymbol{\xi}} \triangleq \hat{\boldsymbol{\xi}} - \boldsymbol{\xi}$ and adaptive term estimation error $\tilde{\varepsilon} = \hat{\varepsilon} - \varepsilon$ converge to zero as $t \to \infty$. According to (14), the observation error $\tilde{\boldsymbol{z}}_r = \hat{\boldsymbol{z}}_r - \boldsymbol{z}_r$ also converges to zero as $t \to \infty$ and the estimation of back EMF can be obtained from (10). The block diagram of the proposed ROAO is shown in Fig. 2.

Remark 1: Although the output matrix $\mathbf{C}_r$ of (11) is constructed by multiplying $\bar{\mathbf{C}}_r$ and $\mathbf{T}^{-1}$, the final calculation result of $\mathbf{C}_r$ does not contain unknown speed information. This implies that the unknown speed information ω_e in the invertible matrix $\mathbf{T}$ does not affect the design or stability of the observer.

Proposition 2: If the stator resistance and inductance deviate from the rated values, the global asymptotic stability of the adaptive observer (16) and (17) proposed in Proposition 1 will weaken to global stability. The upper bound of the observation error $\tilde{\boldsymbol{\xi}}$ depends on the observer gain $k_i (i = 1, 2, 3)$ and the degree of parameter mismatch.

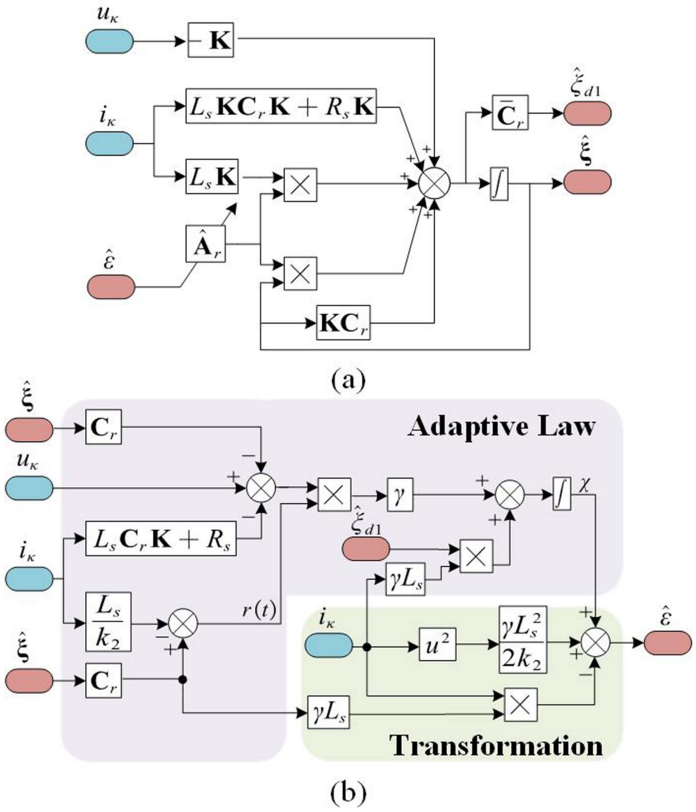

Fig. 2. Block diagram of the proposed ROAO. (a) Adaptive observer. (b) Adaptive term.

B. Stability Analysis Without Parameter Mismatch

To verify the rationality of Proposition 1, the stability of the proposed ROAO without parameter mismatch is analyzed in this part.

The dynamic equation of the observation error $\tilde{\boldsymbol{\xi}}$ is obtained by subtracting (15) from (16) as follows:

$$\dot{\tilde{\boldsymbol{\xi}}} = \mathbf{A}_c\tilde{\boldsymbol{\xi}} + \mathbf{B}_r\tilde{\varepsilon}\left(\hat{\xi}_1 - \frac{L_s}{k_2}i_\alpha\right) \tag{18}$$

where $\mathbf{A}_c = \mathbf{A}_r + \mathbf{K}\mathbf{C}_r = \begin{bmatrix} -k_1/k_2 & 0 \\ \varepsilon - k_1k_3 & -k_2k_3 \end{bmatrix}$ is a Hurwitz matrix and $\mathbf{B}_r = \begin{bmatrix} 0 \\ 1 \end{bmatrix}$. According to (18), the transfer function can be described as follows:

$$\begin{aligned} G(s) &= \mathbf{C}_r\left(s\mathbf{I} - \mathbf{A}_c\right)^{-1}\mathbf{B}_r \\ &= \frac{k_2}{s + k_2k_3}. \end{aligned} \tag{19}$$

Since $G(s)$ is a strictly positive real transfer function. By the Kalman–Yakubovich–Popov (KYP) lemma for passive systems, there exists a matrix $\mathbf{P} = \mathbf{P}^T > 0$ satisfying as follows [37]:

$$\begin{aligned} \mathbf{A}_c^T\mathbf{P} + \mathbf{P}\mathbf{A}_c &= -\mathbf{Q} < 0 \\ \mathbf{P}\mathbf{B}_r &= \mathbf{C}_r^T. \end{aligned} \tag{20}$$

Using the positive definite matrix $\mathbf{P}$ from the KYP lemma, a candidate Lyapunov function is constructed according to (18) as follows:

$$V = \frac{1}{2}\tilde{\boldsymbol{\xi}}^T\mathbf{P}\tilde{\boldsymbol{\xi}} + \frac{1}{2\gamma}\tilde{\varepsilon}^2. \tag{21}$$

Taking the derivative of (21) with respect to time along the trajectory of (18) yields

$$\dot{V} = \frac{1}{2}\tilde{\boldsymbol{\xi}}^T\left(\mathbf{A}_c^T\mathbf{P} + \mathbf{P}\mathbf{A}_c\right)\tilde{\boldsymbol{\xi}} + \tilde{\boldsymbol{\xi}}^T\mathbf{P}\mathbf{B}_r\tilde{\varepsilon}\left(\hat{\xi}_1 - \frac{L_s}{k_2}i_\alpha\right) + \frac{\tilde{\varepsilon}\dot{\tilde{\varepsilon}}}{\gamma}. \tag{22}$$

Substituting (20) into (22) and combining the definitions of y_r and $\boldsymbol{\xi}$ in (11) and (14), (22) can be rewritten as follows:

$$\dot{V} = -\frac{1}{2}\tilde{\boldsymbol{\xi}}^T\mathbf{Q}\tilde{\boldsymbol{\xi}} + \tilde{y}_r\tilde{\varepsilon}\left(\hat{\xi}_1 - \frac{L_s}{k_2}i_\alpha\right) + \frac{\tilde{\varepsilon}\dot{\tilde{\varepsilon}}}{\gamma}. \tag{23}$$

According to (23), the updated law of the adaptive term $\hat{\varepsilon}$ is designed as follows:

$$\dot{\hat{\varepsilon}} = \dot{\tilde{\varepsilon}} = -\gamma\tilde{y}_r\left(\hat{\xi}_1 - \frac{L_s}{k_2}i_\alpha\right) \tag{24}$$

results in

$$\begin{aligned} \dot{V} &= -\frac{1}{2}\tilde{\boldsymbol{\xi}}^T\mathbf{Q}\tilde{\boldsymbol{\xi}} \\ &\leqslant -\frac{1}{2}\lambda_{\min}\left(\mathbf{Q}\right)\tilde{\boldsymbol{\xi}}^T\tilde{\boldsymbol{\xi}}. \end{aligned} \tag{25}$$

By the Lyapunov stability theory, the closed-loop system (18) and (24) is globally stable.

Integrating both sides of (25) gives

$$\int_0^\infty \tilde{\boldsymbol{\xi}}^T\tilde{\boldsymbol{\xi}}dt \leqslant \frac{2\left[V(0) - V(\infty)\right]}{\lambda_{\min}\left(\mathbf{Q}\right)}. \tag{26}$$

Since $V(t) \geqslant 0$ and $\dot{V}(t) \leqslant 0$, the following inequality can be derived:

$$\int_0^\infty \tilde{\boldsymbol{\xi}}^T\tilde{\boldsymbol{\xi}}dt \leqslant \infty. \tag{27}$$

Using Barbalat's lemma, it can be concluded that $\lim_{t\to\infty}\tilde{\boldsymbol{\xi}}(t) = 0$.

Furthermore, according to (18), when $\tilde{\boldsymbol{\xi}}(t) = 0$ and $\hat{\xi}_1 - L_si_\alpha/k_2 \neq 0$ hold, there is no solution can stay identically in $S = \{\tilde{\varepsilon} \in R \mid \tilde{\boldsymbol{\xi}} = 0\}$, other than the trivial solution $\tilde{\varepsilon}(t) \equiv 0$. According to LaSalle's invariance principle [37], it can be concluded that $\lim_{t\to\infty}\tilde{\varepsilon}(t) = 0$.

It is worth mentioning that $\tilde{y}_r = \mathbf{C}_r\tilde{\boldsymbol{\xi}}$ is unavailable in the update law of the adaptive term (24). Combining (7), (11), and (14), rewrites (24) as follows:

$$\begin{aligned} \dot{\hat{\varepsilon}} &= -\gamma\left[\mathbf{C}_r\hat{\boldsymbol{\xi}} - \mathbf{C}_r\left(\boldsymbol{z}_r - L_s\mathbf{K}i_\alpha\right)\right]r(t) \\ &= -\gamma\left(\mathbf{C}_r\hat{\boldsymbol{\xi}} - u_\alpha + L_s\dot{i}_\alpha + R_si_\alpha + L_s\mathbf{C}_r\mathbf{K}i_\alpha\right)r(t) \end{aligned} \tag{28}$$

where $r(t) = \hat{\xi}_1 - L_si_\alpha/k_2$.

In order to avoid using the information about stator current derivatives in the updated law of the adaptive term, a new state

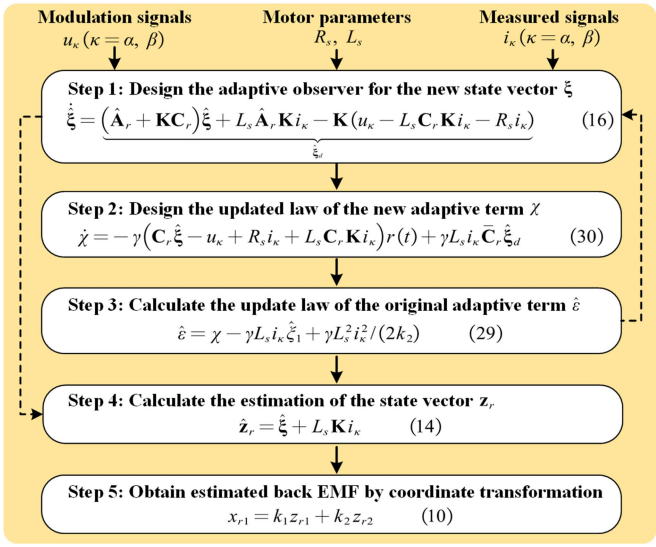

Fig. 3. Final implementation flowchart of the proposed ROAO.

variable is defined as follows:

$$\chi \triangleq \hat{\varepsilon}+\gamma L_si_\alpha\hat{\xi}_1-\frac{\gamma L_s^2}{2k_2}i_\alpha^2. \tag{29}$$

Taking the derivative of (29) with respect to time along the trajectory of (28) yields

$$\begin{aligned}\dot{\chi}&=\dot{\hat{\varepsilon}}+\gamma L_s\dot{i}_\alpha\hat{\xi}_1+\gamma L_si_\alpha\dot{\hat{\xi}}_1-\frac{\gamma L_s^2}{k_2}i_\alpha\dot{i}_\alpha\\&=-\gamma\left(\mathbf{C}_r\hat{\boldsymbol{\xi}}-u_\alpha+R_si_\alpha+L_s\mathbf{C}_r\mathbf{K}i_\alpha\right)r(t)+\gamma L_si_\alpha\bar{\mathbf{C}}_r\hat{\boldsymbol{\xi}}_d,\end{aligned} \tag{30}$$

Combining (21), (24), (25), (29), and (30), the correctness of Proposition 1 is proved.

The final implementation flowchart of the proposed ROAO is illustrated in Fig. 3. In which, only five mathematical operations are required to obtain the estimated back-EMF. In addition, the proposed ROAO clearly does not rely on PLL information and does not require any pure derivation operation.

Remark 2: Many existing works have also made contributions to the stability of PMSM position observers. Table I depicts a comparison between the proposed work with other typical observers. The results indicate that the proposed adaptive observer has advantages in stability properties.

C. Stability Analysis With Parameter Mismatch

The proposed ROAO requires accurate information on the stator resistance and inductance to estimate the rotor speed and position. However, obtaining accurate parameter information in practice is challenging. Therefore, the stability of the proposed ROAO with parameter mismatch is analyzed in this part.

The adaptive observer for (15) under parameter mismatch can be rewritten as follows:

$$\dot{\hat{\boldsymbol{\xi}}}=\left(\hat{\mathbf{A}}_r+\mathbf{K}\mathbf{C}_r\right)\hat{\boldsymbol{\xi}}+L_{s0}\hat{\mathbf{A}}_r\mathbf{K}i_\alpha-\mathbf{K}(u_\alpha-L_{s0}\mathbf{C}_r\mathbf{K}i_\alpha-R_{s0}i_\alpha) \tag{31}$$

TABLE I
COMPARISONS OF PROPOSED WORK WITH OTHER TYPICAL OBSERVERS

Comparative items	Flux observer			Back EMF observer			
	[13]	[15]	[16]	[27], [28], [29], [30]	[34]	[35]	Proposed
Stability properties	GS	GS	GAS	\	LS	LS	GAS
Magnet flux linkage	Need	Need	No need	No need	No need	No need	No need
PE assumption	No	No	Yes	No	No	No	No
Purely integrator	No	No	Yes	No	No	No	No
PLL informationr	No	No	No	Yes	No	No	No

GS: Global Stable. GAS: Global Asymptotic Stable. LS: Local Stable.

where L_{s0} and R_{s0} are the nominal values of the stator resistance and stator inductance, respectively.

The dynamic equation of the observation error $\tilde{\boldsymbol{\xi}}$ can be obtained by subtracting (15) from (31) as follows:

$$\begin{cases}\dot{\tilde{\boldsymbol{\xi}}}=\mathbf{A}_c\tilde{\boldsymbol{\xi}}+\mathbf{B}_r\tilde{\varepsilon}\left(\hat{\xi}_1-\dfrac{L_s}{k_2}i_\alpha\right)+\mathbf{B}_{\Delta1}d_{\Delta1}+\mathbf{B}_rd_{\Delta2}\\ d_{\Delta1}=\left(k_3L_{s\Delta}+\dfrac{k_1L_{s\Delta}}{k_2^2}-k_3L_{s\Delta}-\dfrac{R_{s\Delta}}{k_2}\right)i_\alpha\\ d_{\Delta2}=\left(k_2k_3^2L_{s\Delta}+\dfrac{k_1k_3L_{s\Delta}}{k_2}-\dfrac{\hat{\varepsilon}L_{s\Delta}}{k_2}-k_3R_{s\Delta}\right)i_\alpha\end{cases} \tag{32}$$

where $\mathbf{B}_{\Delta1}=\begin{bmatrix}1\\0\end{bmatrix}$, and $L_{s\Delta}$ and $R_{s\Delta}$ are the deviations between the nominal value and actual values of the stator resistance and stator inductance, which are defined as follows:

$$\begin{cases}L_{s\Delta}=L_{s0}-L_s\\ R_{s\Delta}=R_{s0}-R_s.\end{cases} \tag{33}$$

Taking the derivative of (21) with respect to time along the trajectory of (32) yields

$$\begin{aligned}\dot{V}=&-\frac{1}{2}\tilde{\boldsymbol{\xi}}^T\mathbf{Q}\tilde{\boldsymbol{\xi}}+\tilde{y}_r\tilde{\varepsilon}\left(\hat{\xi}_1-\frac{L_s}{k_2}i_\alpha\right)+\frac{\tilde{\varepsilon}\dot{\tilde{\varepsilon}}}{\gamma}\\&+\tilde{\boldsymbol{\xi}}^T\mathbf{P}\mathbf{B}_{\Delta1}d_{\Delta1}+\tilde{\boldsymbol{\xi}}^T\mathbf{P}\mathbf{B}_rd_{\Delta2}.\end{aligned} \tag{34}$$

Considering the parameter mismatch, the updated law of the adaptive term $\hat{\varepsilon}$ can be redesigned as follows:

$$\dot{\hat{\varepsilon}}=\dot{\tilde{\varepsilon}}=-\gamma\tilde{y}_r\left(\hat{\xi}_1-\frac{L_{s0}}{k_2}i_\alpha\right) \tag{35}$$

results in

$$\dot{V}=-\frac{1}{2}\tilde{\boldsymbol{\xi}}^T\mathbf{Q}\tilde{\boldsymbol{\xi}}+\tilde{\boldsymbol{\xi}}^T\mathbf{P}\mathbf{B}_rd_{\Delta3}+\tilde{\boldsymbol{\xi}}^T\mathbf{P}\mathbf{B}_{\Delta1}d_{\Delta1}+\tilde{\boldsymbol{\xi}}^T\mathbf{P}\mathbf{B}_rd_{\Delta2}. \tag{36}$$

where $d_{\Delta3}=\tilde{\varepsilon}L_{s\Delta}i_\alpha/k_2$.

Under the reasonable assumption that $L_{s\Delta}$ and $R_{s\Delta}$ are bounded, $\mathbf{P}\mathbf{B}_rd_{\Delta3}$, $\mathbf{P}\mathbf{B}_{\Delta1}d_{\Delta1}$, and $\mathbf{P}\mathbf{B}_rd_{\Delta2}$ satisfy

$$\|\mathbf{P}\mathbf{B}_rd_{\Delta3}\|+\|\mathbf{P}\mathbf{B}_{\Delta1}d_{\Delta1}\|+\|\mathbf{P}\mathbf{B}_rd_{\Delta2}\|<g \tag{37}$$

where g is a positive constant.

Substituting (37) into (34) yields

$$\begin{aligned}\dot{V} &\leqslant -\frac{1}{2}\lambda_{\min}(\mathbf{Q})\left\|\tilde{\boldsymbol{\xi}}\right\|^2 + g\left\|\tilde{\boldsymbol{\xi}}\right\| \\ &\leqslant -\left(\frac{1}{2}-\theta\right)\lambda_{\min}(\mathbf{Q})\left\|\tilde{\boldsymbol{\xi}}\right\|^2 + g\left\|\tilde{\boldsymbol{\xi}}\right\| - \theta\lambda_{\min}(\mathbf{Q})\left\|\tilde{\boldsymbol{\xi}}\right\|^2 \\ &\leqslant -\left(\frac{1}{2}-\theta\right)\lambda_{\min}(\mathbf{Q})\left\|\tilde{\boldsymbol{\xi}}\right\|^2 \quad \forall \left\|\tilde{\boldsymbol{\xi}}\right\| \geqslant \frac{g}{\theta\lambda_{\min}(\mathbf{Q})}\end{aligned} \tag{38}$$

where $0 < \theta < 1/2$.

According to (21) and (38), the observation error $\tilde{\boldsymbol{\xi}}$ is bounded with upper bound $g/(\theta\lambda_{\min}(\mathbf{Q}))$, which proves the rationality of Proposition 2.

D. Parameter Design

Based on the above discussions, the parameters to be designed for the proposed ROAO include k_1, k_2, k_3, and γ. The specific design steps and parameter selection method are summarized as follows:

Step 1 : Design $k_i (i = 1, 2, 3)$ in coordinate transformation matrix $\mathbf{T}$ (9) and observer gain matrix $\mathbf{K}$ (12).

First, k_i must be selected as positive real constants to ensure that $\mathbf{A}_c$ in the observation error dynamic equation (18) is a Hurwitz matrix. Second, according to (18), the eigenvalues of the matrix $\mathbf{A}_c$ are $-k_1/k_2$ and $-k_2k_3$, and the values of k_1, k_2, and k_3 can be determined by the relationships as follows:

$$\frac{k_1}{k_2} = k_2k_3 = 2\pi f_{\text{ob}} \tag{39}$$

where f_{ob} is the bandwidth of the back EMF observer, which is recommended to be less than 1/10 of the switching frequency [30].

Step 2 : Choose a positive adaptive gain γ in (17) to ensure the Lyapunov function in (21) is positive definite.

It should be noted that excessively large adaptive gains can deteriorate the control performance or even lead to system instability. Suitable adaptive gains can be selected by trial and error.

Step 3 : Design ROAO based on (16) and (17) to estimate $\boldsymbol{\xi}$.

Step 4 : Calculate the estimation of back EMF $\hat{y}_r$ according to coordinate transformation (10) and (14).

Step 5 : Using PLL to estimate rotor position $\hat{\theta}_e$ and speed $\hat{\omega}_e$, which are used for encoderless vector control.

The overall block diagram of the sensorless speed control based on the proposed ROAO is depicted in Fig. 4.

IV. Simulation and Experimental Results

In this section, the effectiveness of the proposed ROAO is verified through simulations in MATLAB/Simulink platform and experimental tests. The motor under test is an SPMSM fed by a three-phase voltage source inverter (VSI) using the space vector pulse width modulation. Fig. 5 shows a prototype of the SPMSM sensorless speed drive system. The sensorless control algorithm is implemented on a TI TMS320F28335 DSP and

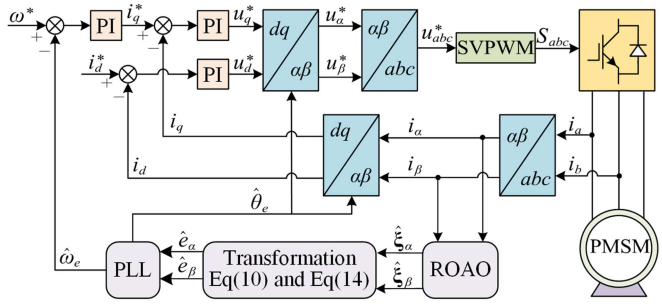

Fig. 4. Overall block diagram of the sensorless speed control based on the proposed ROAO.

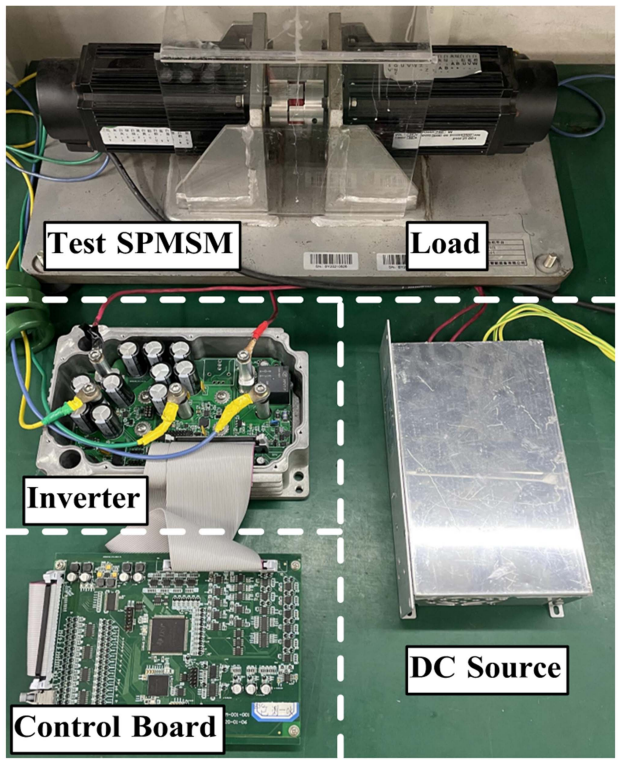

Fig. 5. Prototype of the laboratory platform.

connected to the VSI via a modulation board. A photoelectric encoder is employed to determine the actual position of the rotor, solely used for evaluating the estimated rotor position. The current-to-frequency (IF) starting scheme proposed in [38] is adopted to achieve the startup, transitioning to closed-loop sensorless control at 100 r/min. The specifications of the experimental platform are detailed in Table II. To assess the observation performance of the proposed observer, a comparison was made with the adaptive ESO proposed in [28]. The bandwidth of the speed controller, PLL, and current controllers can be selected as 4, 40, and 400 Hz, respectively. The specific controller and observer parameters are outlined in Table III.

A. Simulation Results

Fig. 6 illustrates the simulation comparison results of the sensorless speed control using different observers when subjected to

TABLE II
PARAMETERS OF THE EXPERIMENTAL SETUP

Symbol	Description	Value
J_n	Moment of inertia	0.0015 [kg·m^2]
B_n	Viscous friction coefficient	0.0002 [N·m·s/rad]
ψ_{fn}	Rotor flux linkage	0.007235 [Wb]
n_p	Number of pole pairs	5
L_s	Stator inductances	0.655 [mH]
R_s	Stator resistance	0.17 [Ω]
V_{dc}	DC-link voltage	24 [V]
f_s	Switching frequency	10 [kHz]
W_{rate}	Rated speed	3000 [r/min]

TABLE III
CONTROLLERS PARAMETERS OF THE EXPERIMENT

Control Structure		Control Parameters
Observer	ROAO	$k_1 = k_3 = 2513$, $k_2 = 1$, $\gamma = 100$
	[28]	$\varepsilon_{\max} = 0.04$, $\omega_{0,\min} = 200$, $\omega_{0,\max} = 3000$
PLL		$k_{p,PLL} = 355.4$, $k_{i,PLL} = 63165$
Speed Controller		$k_{p,\omega} = 0.196$, $k_{i,\omega} = 3.492$
Current Controller		$k_{p,id} = k_{p,iq} = 2.328$, $k_{i,id} = k_{i,iq} = 4137.3$

speed and load variations. Throughout the simulation, the speed of the motor accelerated from 500 to 1000 r/min at 0.1 s, the load stepped from 1 to 2 N.m at 0.15 s, and the speed slowed down from 1000 to 500 r/min at 0.2 s. The results indicate that during the acceleration transient, the maximum back EMF estimation error of the proposed ROAO is 0.1 V, and the maximum position estimation error is 1.7°. In contrast, the adaptive ESO exhibits a maximum back EMF estimation error of up to 0.3 V and a maximum position estimation error of up to 3.5°. Compared with the proposed ROAO under load variation, the maximum back EMF estimation error of the adaptive ESO increases by 270%, and the maximum position estimation error increases by 67%. During the deceleration transient, both the back EMF estimation error and the position estimation error fluctuate more significantly, but those of the proposed ROAO are smaller than those of the adaptive ESO. Based on these findings, it can be concluded that the proposed ROAO exhibits better dynamic performance than the adaptive ESO under load variation and speed variation.

B. Experimental Results

Fig. 7 depicts the experimental comparisons of the steady-state performance with different observers at 500 r/min operating conditions. The signals shown from top to bottom in Fig. 7 include the estimated rotor position, the estimated back EMF, the speed estimation error, and the rotor position estimation error. As shown in Fig. 7(a), the maximum estimation error of rotor position under the proposed ROAO is 2.58° and the maximum estimation error of speed is 4 r/min. In contrast, when using the adaptive ESO, the maximum estimation error

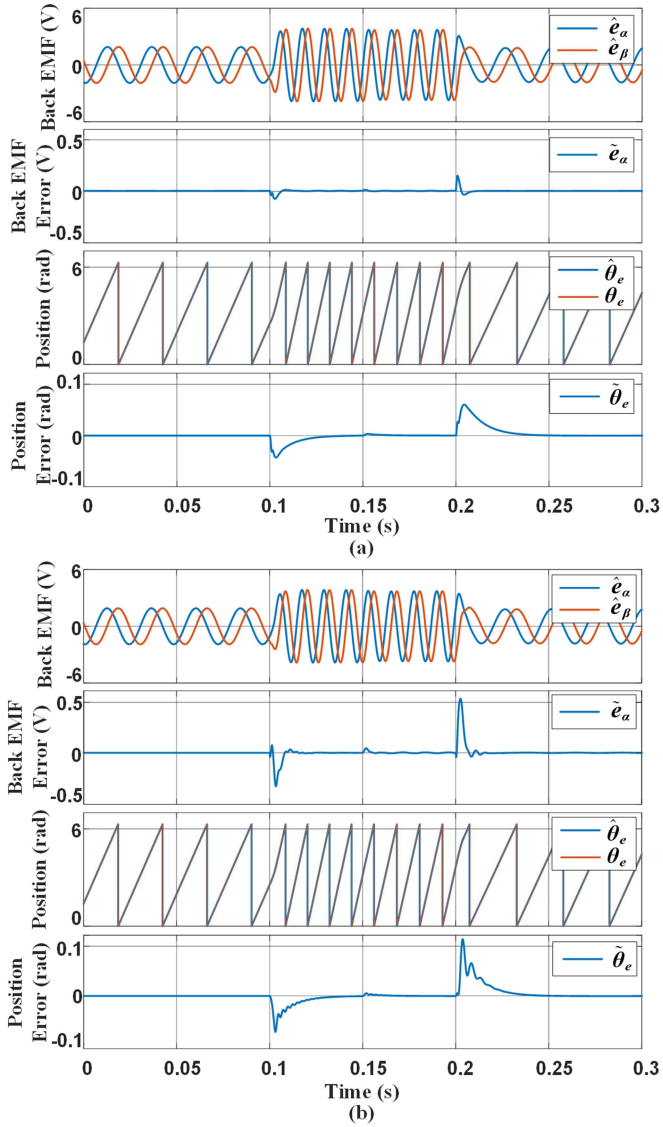

Fig. 6. Simulation comparison results of different observers under the load step and speed variation. (a) Proposed ROAO. (b) Adaptive ESO proposed in [28].

of rotor position increases to 6.3° and the maximum speed estimation error increases to 9 r/min. These experimental results indicate that the proposed ROAO exhibits a smaller steady-state estimation error than the adaptive ESO. This is attributed to the global asymptotic stability of the proposed ROAO, ensuring that the estimation error of the back EMF eventually converges to zero. However, the adaptive ESO can only guarantee stability, and the accuracy of back EMF estimation is highly dependent on the motor speed and the bandwidth of the observer.

The experimental comparison results of sensorless speed control using different observers under load steps are illustrated in Fig. 8. It is evident from the results that both sensorless speed control schemes successfully regulate the motor speed to return to the reference value despite the load torque steps. The settling time of the adaptive ESO is 323 ms, with a speed drop is 52 r/min. The proposed ROAO exhibits a shorter settling time

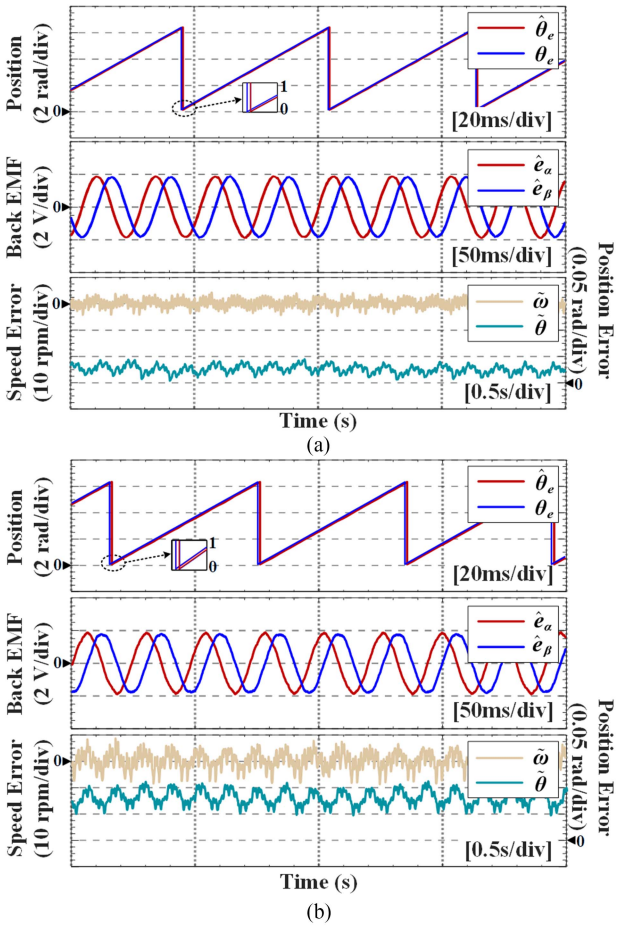

Fig. 7. Experimental comparison results of different observers under the steady-state. (a) Proposed ROAO. (b) Adaptive ESO proposed in [28].

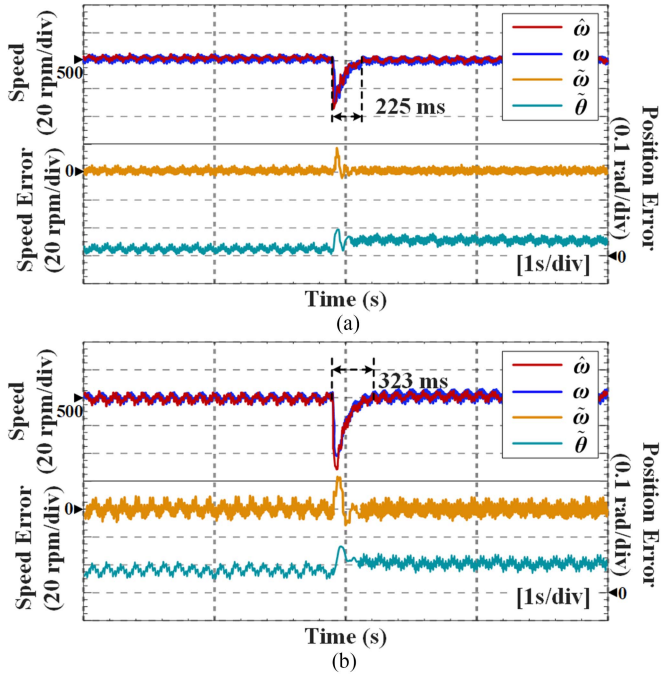

Fig. 8. Experimental comparison results of different observers under the load step. (a) Proposed ROAO. (b) Adaptive ESO proposed in [28].

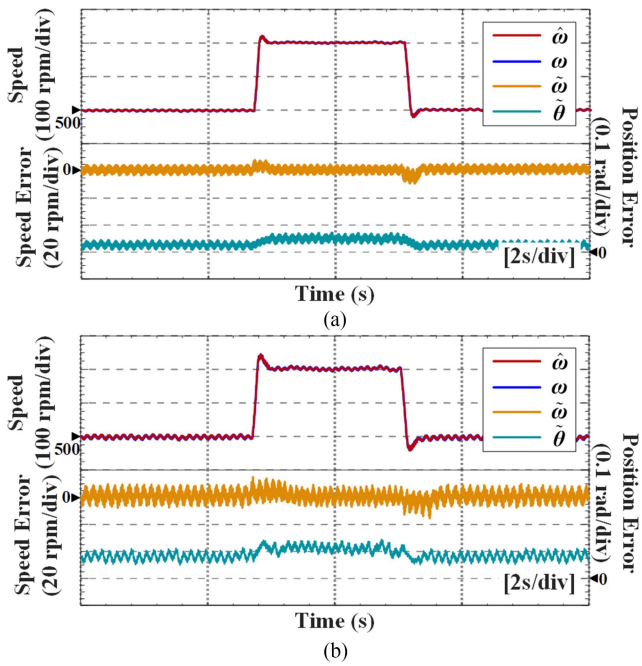

Fig. 9. Experimental comparison results of different observers of the speed reference changes. (a) Proposed ROAO. (b) Adaptive ESO proposed in [28].

(225 ms) and a smaller speed drop (36 r/min) than the adaptive ESO. In addition, the maximum position estimation error using the adaptive ESO reaches up to 9.4°, and the maximum speed estimation error reaches up to 23 r/min. However, the maximum estimation error under the proposed ROAO is 5.2° for position and 14 r/min for speed. It is noteworthy that the rotor position estimation error slightly increases when the load torque steps up. This phenomenon is attributed to environmental noise when the current increases [39]. The performance remains acceptable based on the experimental results.

Fig. 9 displays the experimental comparison results of sensorless speed control using different observers under the speed reference changes from 500 to 700 r/min and back to 500 r/min. Both sensorless speed control schemes effectively regulate the motor speed to the desired value during the speed reference change. During acceleration transient, the adaptive ESO exhibits an overshoot speed of 40 r/min and its settling time is 264.5 ms. The proposed ROAO demonstrates a reduced overshoot speed of only 22 r/min, representing a 45% reduction. Moreover, the settling time under the proposed ROAO is 127.2 ms, showcasing a faster response. Besides, the proposed ROAO outperforms the adaptive ESO with smaller estimation errors of speed and position during the speed reference changes. Specifically, the maximum speed estimation error of the adaptive ESO reaches up to 17 r/min and the maximum position estimation error reaches up to 8.31°. The maximum estimation error of the proposed ROAO is less than 10 r/min for speed and 4.2° for position. Based on the results of Figs. 8 and 9, it can be concluded that the proposed ROAO exhibits better dynamic performance than

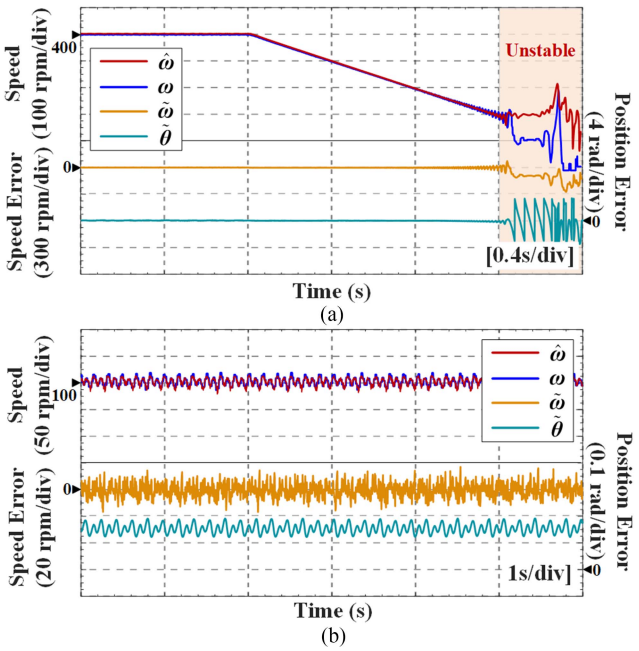

Fig. 10. Experimental results of the speed reference decreasing under the proposed ROAO. (a) 400 to 0 r/min. (b) 100 r/min.

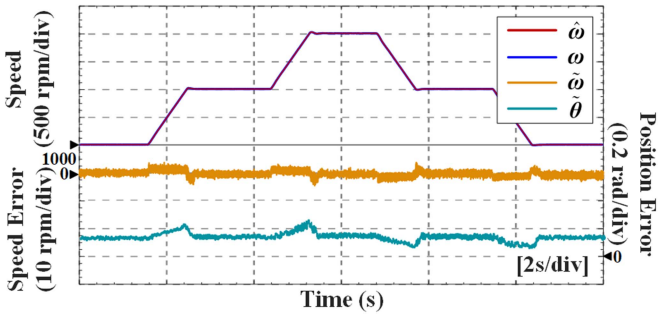

Fig. 11. Experimental results of the proposed ROAO under rated speed with rated load.

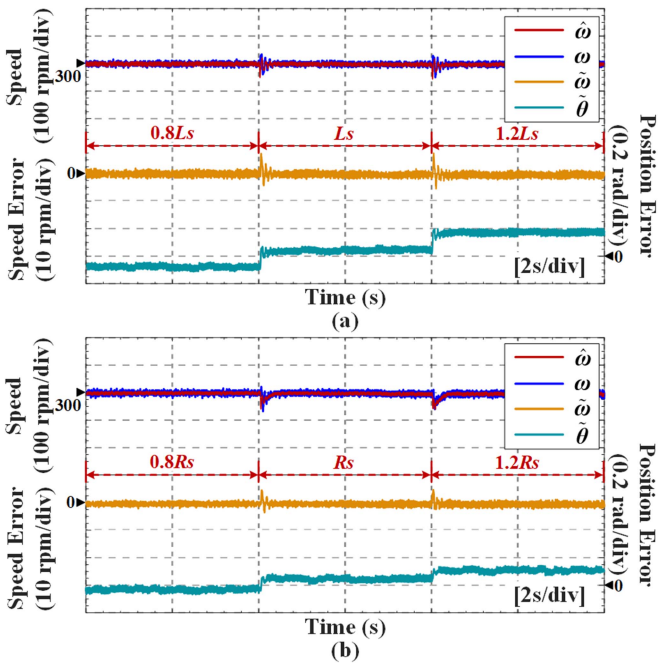

Fig. 12. Experimental results of the proposed ROAO with a 20% parameter mismatch. (a) Stator inductance. (b) Stator resistance.

the adaptive ESO. This is attributed to the fact that the adaptive ESO relies on rotor speed information estimated by the PLL for its design, necessitating a lower bandwidth frequency for the observer compared with the PLL. As a result, the dynamic response of the state observation is limited.

To test the lowest speed that the motor can achieve using the proposed ROAO, Fig. 10(a) presents the experimental results of the speed reference gradually decreasing from 400 to 0 r/min. The experimental results demonstrate that the system remains stable until the speed is reduced to 100 r/min (3.3% of the rated speed), which meets the requirements of most practical applications [29]. In addition, Fig. 10(b) depicts the estimated results of the rotor speed and position at 100 r/min operating conditions. The results indicate that the performance of the observer deteriorates as the motor speed decreases. This phenomenon occurs because the amplitude of the back EMF becomes very small when the motor operates at low speeds, and the performance of the observer is deteriorated by environmental noise and voltage distortion. This limitation is a common shortcoming of back EMF observers. Fig. 11 presents the experimental results of the proposed ROAO under rated speed with rated load. The results indicate that the proposed ROAO maintains good estimation performance at high speeds.

To verify the performance of the proposed observer under the parameter mismatch. Fig. 12(a) and (b) shows the experimental results of the proposed ROAO with a 20% parameter mismatch in stator inductance and resistance at a motor speed of 300 r/min, respectively. The experimental results depict that the maximum speed estimation error is 7.6 r/min under stator inductance mismatch, and the maximum position estimation error is 10.32°. With stator resistance mismatch, the maximum speed estimation error is 4.7 r/min and the maximum position estimation error is 6.19°. Based on the above analysis, it can be concluded that the proposed observer ensures system stability under parameter mismatch, which verifies the rationality of Proposition 2.

Fig. 13 shows the estimated results of the adaptive term under different adaptive gains. The results indicate that the adaptive term can ultimately converge to the true value, which confirms the analytical results in Proposition 1. However, the dynamic performance of the adaptive term is poor. By comparing the experimental results of Fig. 13(a) and (b), it can be concluded that increasing the adaptive gain can improve the dynamic performance of the adaptive term. However, excessively large adaptive gains increase adaptive term chattering and may even lead to system instability. Therefore, the speed estimated by the adaptive term was not used for vector control.

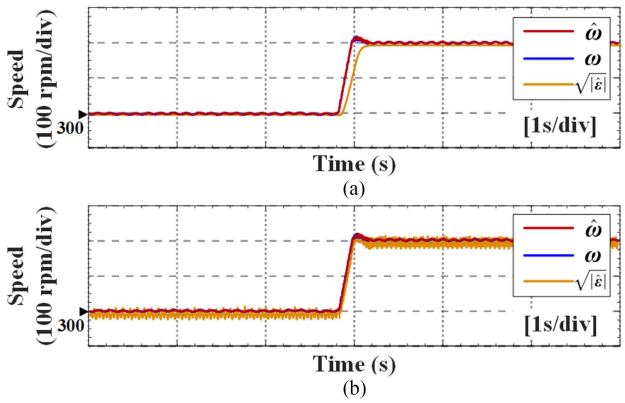

Fig. 13. Experimental results of the adaptive term estimation under different adaptive gains. (a) $\gamma = 1 \times 10^4$. (b) $\gamma = 1 \times 10^6$.

V. Conclusion

This article proposes a sensorless speed control scheme based on ROAO for SPMSM. Unlike most existing back EMF observers, the design of the proposed observer is independent of the PLL. In this case, the bandwidth frequency of the observer is not limited by the PLL, effectively enhancing the dynamic performance of the observer. In addition, the proposed ROAO ensures global asymptotic stability with rigorous proof via the Lyapunov theorem, which provides reasonable guidance on parameter design. Comparisons between the proposed ROAO and the adaptive ESO proposed in [28] are conducted under both steady-state and dynamic conditions. Simulation and experimental results demonstrate that the proposed sensorless speed control strategy has good performance with small estimation errors and fast response.

References

[1] W. Zhu, S. Li, H. Du, and X. Yu, "Nonsmooth observer-based sensorless speed control for permanent magnet synchronous motor," *IEEE Trans. Ind. Electron.*, vol. 69, no. 12, pp. 13514–13523, Dec. 2022.

[2] Y. Jiang, W. Xu, C. Mu, J. Zhu, and R. Dian, "An improved third-order generalized integral flux observer for sensorless drive of PMSMs," *IEEE Trans. Ind. Electron.*, vol. 66, no. 12, pp. 9149–9160, Dec. 2019.

[3] J. Li, Y. Sun, H. Dan, X. Li, F. Zhou, and M. Su, "Adaptive control for SPMSM no need of parameter information but pole pairs," *IEEE Trans. Power Electron.*, vol. 39, no. 3, pp. 3075–3085, Mar. 2024.

[4] G. Wang, M. Valla, and J. Solsona, "Position sensorless permanent magnet synchronous machine drives—A review," *IEEE Trans. Ind. Electron.*, vol. 67, no. 7, pp. 5830–5842, Jul. 2020.

[5] H. Li, X. Zhang, S. Yang, and S. Liu, "Unified graphical model of high-frequency signal injection methods for PMSM sensorless control," *IEEE Trans. Ind. Electron.*, vol. 67, no. 6, pp. 4411–4421, Jun. 2020.

[6] Y.-D. Yoon, S.-K. Sul, S. Morimoto, and K. Ide, "High-bandwidth sensorless algorithm for AC machines based on square-wave-type voltage injection," *IEEE Trans. Ind. Appl.*, vol. 47, no. 3, pp. 1361–1370, May/Jun. 2011.

[7] P. Xu and Z. Zhu, "Carrier signal injection-based sensorless control for permanent-magnet synchronous machine drives considering machine parameter asymmetry," *IEEE Trans. Ind. Electron.*, vol. 63, no. 5, pp. 2813–2824, May 2016.

[8] T.-C. Lin, Z.-Q. Zhu, and J. Liu, "Improved rotor position estimation in sensorless-controlled permanent-magnet synchronous machines having asymmetric-EMF with harmonic compensation," *IEEE Trans. Ind. Electron.*, vol. 62, no. 10, pp. 6131–6139, Oct. 2015.

[9] Y. Park and S.-K. Sul, "Sensorless control method for PMSM based on frequency-adaptive disturbance observer," *IEEE Trans. Emerg. Sel. Topics Power Electron.*, vol. 2, no. 2, pp. 143–151, Jun. 2014.

[10] J. Choi, K. Nam, A. A. Bobtsov, A. Pyrkin, and R. Ortega, "Robust adaptive sensorless control for permanent-magnet synchronous motors," *IEEE Trans. Power Electron.*, vol. 32, no. 5, pp. 3989–3997, May 2017.

[11] H.-S. Kim, S.-K. Sul, H. Yoo, and J. Oh, "Distortion-minimizing flux observer for IPMSM based on frequency-adaptive observers," *IEEE Trans. Power Electron.*, vol. 35, no. 2, pp. 2077–2087, Feb. 2020.

[12] W. Xu, Y. Jiang, C. Mu, and F. Blaabjerg, "Improved nonlinear flux observer-based second-order SOIFO for PMSM sensorless control," *IEEE Trans. Power Electron.*, vol. 34, no. 1, pp. 565–579, Jan. 2019.

[13] R. Ortega, L. Praly, A. Astolfi, J. Lee, and K. Nam, "Estimation of rotor position and speed of permanent magnet synchronous motors with guaranteed stability," *IEEE Trans. Control Syst. Technol.*, vol. 19, no. 3, pp. 601–614, May 2011.

[14] J. Lee, J. Hong, K. Nam, R. Ortega, L. Praly, and A. Astolfi, "Sensorless control of surface-mount permanent-magnet synchronous motors based on a nonlinear observer," *IEEE Trans. Power Electron.*, vol. 25, no. 2, pp. 290–297, Feb. 2010.

[15] J. Liu and Y. Zhang, "Performance improvement of nonlinear flux observer for sensorless control of PMSM," *IEEE Trans. Ind. Electron.*, vol. 70, no. 12, pp. 12014–12023, Dec. 2023.

[16] A. A. Bobtsov, A. A. Pyrkin, R. Ortega, S. N. Vukosavic, A. M. Stankovic, and E. V. Panteley, "A robust globally convergent position observer for the permanent magnet synchronous motor," *Automatica*, vol. 61, pp. 47–54, 2015.

[17] K. Prabhakaran and A. Karthikeyan, "Electromagnetic torque-based model reference adaptive system speed estimator for sensorless surface mount permanent magnet synchronous motor drive," *IEEE Trans. Ind. Electron.*, vol. 67, no. 7, pp. 5936–5947, Jul. 2020.

[18] O. C. Kivanc and S. B. Ozturk, "Sensorless PMSM drive based on stator feedforward voltage estimation improved with MRAS multiparameter estimation," *IEEE/ASME Trans. Mechatron.*, vol. 23, no. 3, pp. 1326–1337, Jun. 2018.

[19] T. Shi, Z. Wang, and C. Xia, "Speed measurement error suppression for PMSM control system using self-adaption Kalman observer," *IEEE Trans. Ind. Electron.*, vol. 62, no. 5, pp. 2753–2763, May 2015.

[20] V. Smidl and Z. Peroutka, "Advantages of square-root extended Kalman filter for sensorless control of AC drives," *IEEE Trans. Ind. Electron.*, vol. 59, no. 11, pp. 4189–4196, Nov. 2012.

[21] Y. Wang, Y. Xu, and J. Zou, "Sliding-mode sensorless control of PMSM with inverter nonlinearity compensation," *IEEE Trans. Power Electron.*, vol. 34, no. 10, pp. 10206–10220, Oct. 2019.

[22] Z. Qiao, T. Shi, Y. Wang, Y. Yan, C. Xia, and X. He, "New sliding-mode observer for position sensorless control of permanent-magnet synchronous motor," *IEEE Trans. Ind. Electron.*, vol. 60, no. 2, pp. 710–719, Feb. 2013.

[23] C. Gong, Y. Hu, J. Gao, Y. Wang, and L. Yan, "An improved delay-suppressed sliding-mode observer for sensorless vector-controlled PMSM," *IEEE Trans. Ind. Electron.*, vol. 67, no. 7, pp. 5913–5923, Jul. 2020.

[24] Z. Chen, X. Zhang, H. Zhang, C. Liu, and G. Luo, "Adaptive sliding mode observer-based sensorless control for SPMSM employing a dual-PLL," *IEEE Trans. Transport. Electrific.*, vol. 8, no. 1, pp. 1267–1277, Mar. 2022.

[25] W. Xu, S. Qu, L. Zhao, and H. Zhang, "An improved adaptive sliding mode observer for middle-and high-speed rotor tracking," *IEEE Trans. Power Electron.*, vol. 36, no. 1, pp. 1043–1053, Jan. 2021.

[26] Z. Yin, Y. Zhang, X. Cao, D. Yuan, and J. Liu, "Estimated position error suppression using novel PLL for IPMSM sensorless drives based on full-order SMO," *IEEE Trans. Power Electron.*, vol. 37, no. 4, pp. 4463–4474, Apr. 2022.

[27] P. Kshirsagar et al., "Implementation and sensorless vector-control design and tuning strategy for SMPM machines in fan-type applications," *IEEE Trans. Ind Appl.*, vol. 48, no. 6, pp. 2402–2413, Nov./Dec. 2012.

[28] F. Jiang et al., "Robustness improvement of model-based sensorless SPMSM drivers based on an adaptive extended state observer and an enhanced quadrature PLL," *IEEE Trans. Power Electron.*, vol. 36, no. 4, pp. 4802–4814, Apr. 2021.

[29] S. Chen, W. Ding, R. Hu, X. Wu, and S. Shi, "Sensorless control of PMSM drives using reduced order quasi resonant-based ESO and Newton–Raphson method-based PLL," *IEEE Trans. Power Electron.*, vol. 38, no. 1, pp. 229–244, Jan. 2023.

[30] D. Bao, X. Pan, Y. Wang, X. Wang, and K. Li, "Adaptive synchronous-frequency tracking-mode observer for the sensorless control of a surface PMSM," *IEEE Trans. Ind. Appl.*, vol. 54, no. 6, pp. 6460–6471, Nov./Dec. 2018.

[31] Y. Cui, Z. Yin, P. Luo, D. Yuan, and J. Liu, "Linear active disturbance rejection control of IPMSM based on quasi-proportional resonance and disturbance differential compensation linear extended state observer," *IEEE Trans. Ind. Electron.*, vol. 71, no. 10, pp. 11910–11924, Oct. 2024.
[32] A. Tilli, A. Bosso, and C. Conficoni, "Towards sensorless observers for sinusoidal electric machines with variable speed and no mechanical model: A promising approach for PMSMs," *Syst. Control Lett.*, vol. 123, pp. 16–23, 2019.
[33] G. Wang, H. Zhan, G. Zhang, X. Gui, and D. Xu, "Adaptive compensation method of position estimation harmonic error for EMF-based observer in sensorless IPMSM drives," *IEEE Trans. Power Electron.*, vol. 29, no. 6, pp. 3055–3064, Jun. 2014.
[34] S. Po-Ngam and S. Sangwongwanich, "Stability and dynamic performance improvement of adaptive full-order observers for sensorless PMSM drive," *IEEE Trans. Power Electron.*, vol. 27, no. 2, pp. 588–600, Feb. 2012.
[35] C. J. Volpato Filho and R. P. Vieira, "Adaptive full-order observer analysis and design for sensorless interior permanent magnet synchronous motors drives," *IEEE Trans. Ind. Electron.*, vol. 68, no. 8, pp. 6527–6536, Aug. 2021.
[36] K.-B. Lee and F. Blaabjerg, "Reduced-order extended Luenberger observer based sensorless vector control driven by matrix converter with nonlinearity compensation," *IEEE Trans. Ind. Electron.*, vol. 53, no. 1, pp. 66–75, Feb. 2006.
[37] H. K. Khalil, *Nonlinear Systems Third Edition*. Upper Saddle River NJ, USA: Prentice Hall Inc, 2002.
[38] Z. Wang, K. Lu, and F. Blaabjerg, "A simple startup strategy based on current regulation for back-EMF-based sensorless control of PMSM," *IEEE Trans. Power Electron.*, vol. 27, no. 8, pp. 3817–3825, Aug. 2012.
[39] X. Song, J. Fang, B. Han, and S. Zheng, "Adaptive compensation method for high-speed surface PMSM sensorless drives of EMF-based position estimation error," *IEEE Trans. Power Electron.*, vol. 31, no. 2, pp. 1438–1449, Feb. 2016.

Jiong Li was born in Hunan, China, in 1998. He received the B.S. degree in resource exploration engineering in 2020 from Central South University, Changsha, China, where he is currently working toward the Ph.D. degree in electrical engineering.

His current research interests include control of PMSM and stability analysis of power electronics devices.

Yao Sun (Member, IEEE) was born in Hunan, China, in 1981. He received the B.S. and M.S. degrees in automation, and the Ph.D. degree in control science and engineering from the School of Information Science and Engineering, Central South University, Changsha, China, in 2004, 2007, and 2010, respectively.

His research interests include matrix converter, micro-grid, and wind energy conversion systems.

Jianheng Lin (Member, IEEE) was born in Fujian, China, in 1994. He received the B.S. degree in electrical engineering from Jimei University, Xiamen, China, in 2016, and the Ph.D. degree in control science and engineering from Central South University, Changsha, China, in 2022.

He is currently a Lecturer with the School of Automation, Central South University. His research interests include modeling, control, and measurement of power-electronized power systems.

Xing Li was born in Hunan, China, in 1988. She received the B.S. degrees in automation, and the Ph.D. degree in control science and engineering from the School of Information Science and Engineering, Central South University, Changsha, China, in 2009, and 2014, respectively.

She is currently an Associate Professor with the College of Electrical and Information Engineering, Hunan University, Changsha, China. Her research interests include power electronic converters and wind energy conversion systems.

Feng Zhou (Member, IEEE) received the B.Eng., M.Eng., and Ph.D. degrees in control science and engineering from Central South University, Changsha, China, in 2009, 2012, and 2017, respectively.

He is currently an Associate Professor with the School of Electronic Information and Electrical Engineering, Changsha University, Changsha. His main research focuses on high-performance predictive control technology for motor drive systems.

Hanbing Dan (Senior Member, IEEE) was born in Hubei, China, in 1991. He received the B.S. degree in automation, and the Ph.D. degree in control science and engineering from Central South University, Changsha, China, in 2012, and 2017, respectively.

He was a visiting Researcher with the Faculty of Engineering, University of Nottingham, Nottingham, U.K. during 2017. Since 2018, he has been with the School of Automation, Central South University, Changsha, China, where he is currently an Associate Professor. His research interests include power converter and motor control.